DIFFUSE SUNLIGHT BASED CALIBRATION OF THE WATER VAPOR CHANNEL IN THE UPC RAMAN LIDAR

Constantino Muñoz-Porcar[1]*, Adolfo Comeron[1], Michaël Sicard[1], Ruben Barragan[1], David Garcia-Vizcaino[1], Alejandro Rodríguez-Gómez[1], Francesc Rocadenbosch[1]

*[1]Universitat Politècnica de Catalunya, Barcelona, Spain, *constan@tsc.upc.edu*
[2]Ciències i Tecnologies de l'Espai - Centre de Recerca de l'Aeronàutica i de l'Espai / Institut d'Estudis Espacials de Catalunya (CTE-CRAE / IEEC), Universitat Politècnica de Catalunya, Barcelona, Spain

ABSTRACT

A method for determining the calibration factor of the water vapor channel of a Raman lidar, based on zenith measurements of diffuse sunlight and on assumptions regarding some system parameters and Raman scattering models, has been applied to the lidar system of Universitat Politècnica de Catalunya (UPC; Technical University of Catalonia, Spain). Results will be analyzed in terms of stability and comparison with typical methods relying on simultaneous radiosonde measurements.

1 WATER VAPOR MIXING RATIO

The water vapor mixing ratio (*WVMR*) in the atmosphere is defined as the ratio between the water vapor mass in a given volume and the mass of the rest of the volume. As the water vapor mass is always going to be much lesser than the mass of the rest of molecules in the volume, this latter mass can be approximated by the mass of the dry air. Taking into account, moreover, that the molecular weight of water molecules is 18, the mean molecular weight of the air is 28.96 (page 4 of ref. [1]) and that the nitrogen (N_2) volume proportion in the air (hence the proportion of its molecule number concentration) is 78.08%, the mixing ratio can be expressed as

$$\omega = \frac{0.7808 \times 18 \times N_W}{28.96 \times N_N}, \qquad (1)$$

where N_W is the number concentration of water vapor molecules and N_N the number concentration of nitrogen molecules.

2 WATER VAPOR MIXING RATIO FROM RAMAN LIDAR SIGNALS

The detected signal voltage (or the count rate per bin) from a given range R in the nitrogen and water vapor Raman channels of a lidar instrument is given by the lidar equation:

$$S_X(R) = \frac{E\, A_r\, c\, K_X O_X(R) N_X(R) \frac{\partial \sigma_{X\,eff}}{\partial \Omega}}{2R^2} \exp\left\{-\int_0^R \left[\alpha(r,\lambda_0) + \alpha(r,\lambda_X)\right] dr\right\}, \qquad (2)$$

where X is either W or N (referring respectively to water vapor and nitrogen channels); E is the emitted pulse energy at λ_0 (355 nm in our case); A_r is the effective receiving area; c is the speed of light; K_X is, for each detected wavelength, a system constant taking into account the end-to-end transmittance of the receiving optics, the photodetector responsivity and a transducer constant; $O_X(R)$ is the overlap function profile; the exponential term takes into account the extinction along the propagation path of both the emitted pulse (λ_0) and the scattered Raman-shifted radiation (λ_X); $\partial\sigma_{X\,eff}/\partial\Omega$ is the effective differential Raman backscatter cross-section of the species, which takes into account the frequency selection produced in the narrowband interference filters (see Eq. (6)) [2]. No temperature dependence of Raman scattering has been considered in this formulation.

From Eqs. (1) and (2):

$$\omega(R) = 0.4853 \times \frac{K_N}{K_W} \frac{O_N(R)}{O_W(R)} \frac{\frac{\partial \sigma_{N\,eff}}{\partial \Omega}}{\frac{\partial \sigma_{W\,eff}}{\partial \Omega}} \times \frac{S_W(R)}{S_N(R)} \times \exp\left\{\int_0^R \left[\alpha(r,\lambda_W) - \alpha(r,\lambda_N)\right] dr\right\}. \qquad (3)$$

Differences in transmission at the Raman frequencies accounted for in the exponential term can be neglected in common situations: Rayleigh contribution, computed using atmospheric models,

results in differences below 3% for altitudes where water vapor content is meaningful, while differences in aerosol extinction would only produce significant errors in heavily aerosol loaded atmospheres ($AOD > 2$) [3]. If, moreover, identical overlap functions are assumed, the *WVMR* can be obtained multiplying the ratio between the signal profiles corresponding to water vapor and nitrogen Raman channels by a calibration factor that has to be obtained for each lidar instrument. This factor depends on both the effective Raman backscatter cross-sections and the system constants in each channel:

$$\omega(R) = F_{CAL}\frac{S_W(R)}{S_N(R)}, \tag{4}$$

with

$$F_{CAL} = 0.4853 \times \frac{\dfrac{\partial\sigma_{N\,eff}}{\partial\Omega}\dfrac{K_N}{K_W}}{\dfrac{\partial\sigma_{W\,eff}}{\partial\Omega}}. \tag{5}$$

The effective Raman backscatter cross-section can be calculated in each channel as a summation of the spectral lines weighed by the normalized transmission of the corresponding interference filter at each frequency [2]:

$$\frac{\partial\sigma_{X\,eff}}{\partial\Omega} = \sum_i \frac{\partial\sigma_X(\lambda_i)}{\partial\Omega} t_X(\lambda_i), \tag{6}$$

where λ_i is the wavelength corresponding to each line of the Raman spectrum, $\partial\sigma_X(\lambda_i)/\partial\Omega$ and $t_X(\lambda_i)$ being respectively the corresponding differential backscatter cross-section and the normalized transmission function of the interference filter for the specie *X*.

Filter transmission functions have been provided by the filter manufacturer, while differential Raman cross sections for each spectral line have been computed following [4] in the case of water vapor and [5] in the case of Nitrogen. As an example, Figure 1 shows the relative distribution of the spectral lines for nitrogen at 275K and the transmission curve of the corresponding interference filter used in the UPC system. In our case, the effective differential Raman backscattered cross-sections have resulted 2.41×10^{-34} m^2/sr for nitrogen (computed between 384 and 390 nm) and 7.03×10^{-34} m^2/sr for water vapor (computed between 405 and 410 nm). The ratio between both effective cross-sections appearing in Eq. (5) is thus 0.34.

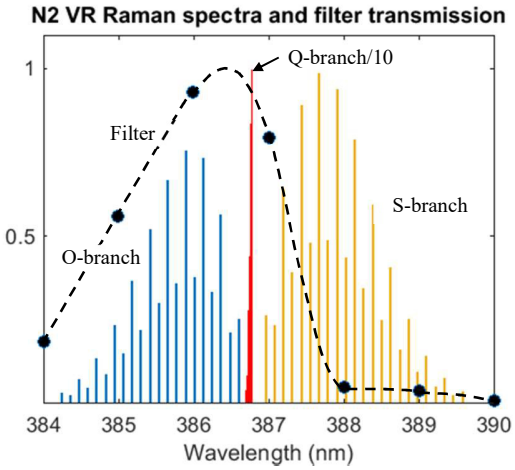

Figure 1 N_2 Raman spectra and interference filter transmission curve.

3 CALIBRATION FACTOR USING DIFFUSE SUNLIGHT RADIATION

The ratio between system constants K_X needed in Eq. (5) to find the calibration factor can be derived from the measurement of diffuse sunlight radiation in N_2 and water vapor channels of the lidar instrument [6]. Once the "dark" offset –due to electronics and photodetector dark current in the case of an analog channel, or to dark counts for a photoncounting channel– has been removed from the detected signal, we obtain a background-radiation induced DC voltage S_{BX} that is

$$S_{BX} = K_X A_r \Omega_X B_X L_{\lambda X}, \tag{7}$$

where *X* stands again for either N_2 or H_2O, Ω_X is the receiver field of view for either the N_2 or the H_2O Raman channel, B_X is the interference filter effective bandwidth, and $L_{\lambda X}$ is the spectral radiance at the corresponding Raman-shifted wavelength. Then we have

$$\frac{S_{BN}}{S_{BW}} = \frac{K_N}{K_W}\frac{\Omega_N}{\Omega_W}\frac{B_N}{B_W}\frac{L_{\lambda N}}{L_{\lambda W}}. \tag{8}$$

Eq. (8) shows that if the ratios between Ω_X, B_X and $L_{\lambda X}$ are known, the ratio between the system constants K_X, required in Eq. (5) for calculating the calibration factor F_{CAL}, can be obtained by computing the ratio of the measured background-radiation induced offsets S_{BX}:

$$\frac{K_N}{K_W} = \frac{\Omega_W}{\Omega_N}\frac{B_W}{B_N}\frac{L_{\lambda W}}{L_{\lambda N}}\frac{S_{BN}}{S_{BW}} \quad (9)$$

We have assumed as an approximation that the field of view in both channels is the same. Regarding the data provided by the manufacturer of the filters it has been also assumed that the effective bandwidths ratio B_W/B_N is 0.91. The ratio between spectral radiances, which depends on the day of the year, the time and the aerosol loading conditions, has been estimated for each individual calibration using a radiative transfer model (GAME [7]) and auxiliary measurements (lidar, sun photometer, radiosondes, etc.). Finally, the background-induced signals S_{BN} and S_{BW} can be obtained either directly from diffuse sunlight radiation measurements or from lidar signals at 25-30 km, where backscatter contribution can be assumed to be negligible.

A set of calibration measurements during 2016 has been used to obtain the ratio of background photo-counting mode signals in the lidar instrument. Simulations to obtain in each case the ratio of spectral radiances have been also performed. With these results and with the rest of estimated parameters, the calibration factor F_{CAL} has been calculated in each case using Eqs. (5) and (9). Figure 2 shows the resulting values for a set of 18 calibrations performed in February 23th between 8:00 UTC and 17:30 UTC. The relative detected illumination intensity in each measurement is plotted too. In this case background offsets where obtained from lidar signals between 25 and 30 km. Table 1 Calibrations between Feb. and June, 2016.

(N: Number of calibrations; SD: standard deviation)
**Background values from lidar signals at 25 - 30 km*

Date	*N*	F_{CAL}	*SD*
22/02/2016*	13	0.230	2.56%
23/02/2016*	18	0.225	2.10%
31/03/2016*	13	0.206	3.31%
11/04/2016	1	0.208	-
13/04/2016	1	0.207	-
18/04/2016	1	0.205	-
03/05/2016	1	0.207	-
20/06/2016	1	0.209	-
23/06/2016	9	0.209	1.47%

4 COMPARISON WITH CALIBRATIONS USING RADIOSONDE DATA

shows the results corresponding to other calibrations between February and June 2016.

All sets of multiple calibrations performed in the same day from dawn to sunset (22/02, 23/02, 31/03 and 20/06) show no significant dependence on illumination intensity or solar zenith angle. Results show in general good short-term stability: The relative standard deviation during the 7 dates of calibrations between 31/03 and 23/06 is only 0.64%. On the other hand, between calibrations made in February and all the rest, starting in 31/03 and ending in 23/06, a significant decrease of the calibration factor can be observed (~10%). This change, produced by at the moment unidentified changes in the instrument conditions, indicate that periodic calibrations should be performed.

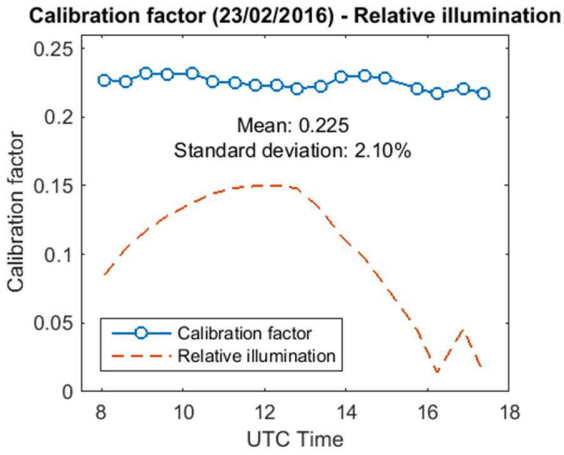

Figure 2 Calibration factor F_{CAL} (February 23th, 2016). Relative illumination is also plotted.

Table 1 Calibrations between Feb. and June, 2016.
(N: Number of calibrations; SD: standard deviation)
**Background values from lidar signals at 25 - 30 km*

Date	*N*	F_{CAL}	*SD*
22/02/2016*	13	0.230	2.56%
23/02/2016*	18	0.225	2.10%
31/03/2016*	13	0.206	3.31%
11/04/2016	1	0.208	-
13/04/2016	1	0.207	-
18/04/2016	1	0.205	-
03/05/2016	1	0.207	-
20/06/2016	1	0.209	-
23/06/2016	9	0.209	1.47%

5 COMPARISON WITH CALIBRATIONS USING RADIOSONDE DATA

The calibration factor F_{CAL} can be also obtained by comparison with simultaneous measurements from a reference instrument [3]. In our case, 150 minutes, night-time lidar measurements and almost collocated, simultaneous radiosondes data have

been used to estimate the calibration factor of the lidar instrument in dates close to cases in section 3. The estimated calibration factor has been obtained from the Raman signals $S_N(R)$, $S_W(R)$ and the *WVMR* values provided by the radiosonde $\omega_{RS}(R)$, which is taken as reference. From Eq. (4):

$$F_{\mathrm{CAL}} = \frac{\omega_{RS}(R)\, S_N(R)}{S_W(R)} \qquad (10)$$

Two cases have been studied: The first one in January 28th, 2016, which is relatively close to February background-based calibrations, and the second one in June 20th, which is coincident with another one. Figure 3 shows, in the latter case, the calibration factor as a function of the altitude where the estimation has been computed and its mean value and standard deviation within a useful calibration range. The upper limit of this useful range is determined by the region where water vapor signal is strong enough for good estimations. Lidar and radiosonde profiles are usually not coincident either in the lowest part of the atmosphere, which obliges to limit also the minimum height of the calibration range. Table 2 summarizes the results of both tests, which show good agreement with the ones obtained using diffuse sunlight calibrations.

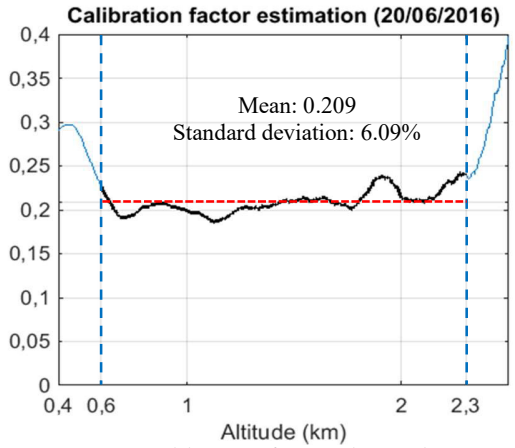

Figure 3 Calibration factor obtained using a radiosonde as reference instrument (20/06/2016).

Table 2 Comparison between calibrations.

Radiosonde			Diffuse sunlight	
Date	**Mean**	***SD***	**Date**	F_{CAL}
28/01/2016	0.226	8.32%	22/02/2016	0.230
20/06/2016	0.209	6.09%	20/06/2016	0.209

6 CONCLUSIONS

The calibration factor required for water vapor mixing ratio measurements has been estimated from direct measurements of diffuse sunlight radiation. Results show good short-term stability, no significant dependence on illumination intensity or solar zenith angle and good agreement with the calibration factor obtained with the classical method based on the use of simultaneous radiosonde measurements. Mid-term changes of the calibration factor reveal the need of performing periodic calibrations of the instrument to assure accurate water vapor measurements. The method can be therefore used as an easy and reliable alternative to the typical calibration relying on radiosondes.

ACKNOWLEDGEMENTS

This work has received funding from the European Union H2020 programme under ACTRIS-2 project (GA 654109), the Spanish Ministry of Economy and Competitiveness – European Regional Development Funds under TEC2015-63832-P project, and from Generalitat de Catalunya (Grup de Recerca Consolidat) 2014-SGR-583.

References

[1] R. M. Measures, Laser remote sensing: fundamentals and applications. Malabar, Fla.: Krieger, 1992.

[2] D. D. Venable et al., Lamp mapping technique for independent determination of the water vapor mixing ratio calibration factor for a Raman lidar system., Appl. Opt., 50 (23), pp. 4622–4632, 2011.

[3] I. Mattis et al., Relative-humidity profiling in the troposphere with a Raman lidar., Appl. Opt., 41(30), pp. 6451–62, 2002.

[4] G. Avila et al., The Raman spectra and cross-sections of H2O, D2O, and HDO in the OH/OD stretching regions, J. Mol. Spectrosc., 228(1), pp. 38–65, 2004.

[5] F. Liu and F. Yi, Lidar-measured atmospheric N_2 vibrational-rotational Raman spectra and consequent temperature retrieval, Opt. Express, 22(23), p. 27833, 2014.

[6] V. Sherlock et al., Methodology for the independent calibration of Raman backscatter water-vapor lidar systems, Appl. Opt., 38(27), pp. 5816–5837, 1999.

[7] P. Dubuisson et al., Water vapor retrieval over ocean using near-infrared radiometry, J. Geophys. Res., 109(D19), Oct. 2004.